JOURNAL OF GEOPHYSICAL RESEARCH, VOL. 92, NO. B1, PAGES 393–405, JANUARY 10, 1987

P Wave Velocity Variations in the Coso Region, California, Derived From Local Earthquake Travel Times

MARIANNE C. WALCK

Geophysics Division, *Sandia National Laboratories, Albuquerque, New Mexico*

ROBERT W. CLAYTON

Seismological Laboratory, California Institute of Technology, Pasadena, California

Inversion of 4036 *P* wave travel time residuals from 429 local earthquakes using a tomographic scheme provides information about three-dimensional upper crustal velocity variations in the Indian Wells Valley–Coso region of southeastern California. The residuals are calculated relative to a Coso-specific velocity model, corrected for station elevation, weighted, and back-projected along their ray paths through models defined with layers of blocks. Slowness variations in the surface layer reflect local geology, including slow velocities for the sedimentary basins of Indian Wells and Rose valleys and relatively fast velocities for the Sierra Nevada and Argus Mountains. In the depth range of 3–5 km the inversion images an area of reduced compressional velocity in western and northern Indian Wells Valley but finds no major velocity variations beneath the Coso volcanic field to the north. These results are consistent with a recent study of anomalous shear wave attenuation in the Coso region. Between 5 and 10 km depth, low-velocity areas (7% slow) appear at the southern end of the Coso volcanics, reaching east to the Coso Basin. Numerical tests of the inversion's resolution and sensitivity to noise indicate that these major anomalies are significant and well-resolved, while other apparent velocity variations in poorly sampled areas are probably artifacts. The seismic data alone are not sufficient to uniquely characterize the physical state of these low-velocity regions. Because of the Coso region's history of Pleistocene bimodal volcanism, high heat flow, geothermal activity, geodetic deformation, and seismic activity, one possibility is to link the zones of decreased *P* velocity to contemporary magmatic activity.

INTRODUCTION

Tomographic inversion of compressional wave travel times is a computationally efficient technique for determining three-dimensional velocity variations in the subsurface beneath a seismic array. Depending on the station separation and the phases used, seismic tomography can be utilized to image heterogeneities with a wide variety of scale lengths. R. P. Comer and R. W. Clayton (unpublished manuscript, 1986) invert the International Seismological Centre (ISC) teleseismic *P* arrival data set for mantle heterogeneities on a global scale. Teleseismic data recorded at the densely spaced California Institute of Technology (Caltech)/U.S. Geological Survey (USGS) southern California seismic network enable *Humphreys et al.* [1984] to investigate the upper mantle at a regional level using tomographic techniques. Crustal structure in southern California is examined by *Hearn and Clayton* [1986*a*, *b*], using the regional crust and mantle phases *Pg* and *Pn*. With arrival time data from local events, *Kissling et al.* [1984] conduct a travel time study to detail the upper crustal velocities in the Long Valley caldera of eastern California. They identify areas of low *P* wave velocity with dimensions of only a few kilometers which may be related to a silicic magma chamber beneath the caldera.

The present study applies seismic tomography to local earthquake data from the tectonically active Coso region of southeastern California in order to spatially locate any upper crustal velocity anomalies. Like Long Valley, the Coso area is one of young volcanism, where small magma chambers may be present [e.g., *Bacon*, 1982; *Lanphere et al.*, 1975]. Located in a transitional regime between the southern Sierra Nevada mountains to the west and the Basin and Range province to the east, the Coso area is dominated by a Pleistocene rhyolite dome field, flanking basalt flows, and cinder cones [*Bacon*, 1982; *Duffield*, 1975; *Duffield et al.*, 1981]. Deep alluvium-filled valleys are present on three sides of the volcanic area. Rose Valley separates the Coso volcanics from the Sierra Nevada, while Indian Wells Valley and the Coso Basin lie to the south and southeast, respectively (see Figure 1).

The Coso volcanic field sits astride a structurally high block composed of Sierra-type granitic rocks [*Duffield*, 1975; *Duffield and Bacon*, 1981; *Bacon et al.*, 1980]. Both strike-slip and normal faulting styles are observed in the region. *Weaver and Hill* [1979] suggest that the Coso volcanics represent a local spreading center and is in an extensional state, which would allow magma to rise near the surface. Geodetic data [*Savage et al.*, 1975] support current modest extension for the Coso region [*Roquemore*, 1981] in accord with the *Weaver and Hill* [1979] hypothesis. The presence of regional arcuate structures sparked a controversy about Coso's fundamental structural style: *Austin et al.* [1971] and *Duffield* [1975] favor a caldera-like structure, while *Roquemore* [1981] maintains that the arcuate features result from stresses induced by strike-slip faulting. The Coso region has never produced a large ash flow eruption; thus the silicic magma may be deep [*Bacon et al.*, 1980] or the area could still be in a precaldera state [*Duffield*, 1975].

The remnants of the Pleistocene volcanic activity are manifested in surface expressions of geothermal activity near the center of the volcanic field. There are active fumaroles and hot springs, and *Combs* [1980] documents extremely high heat flow values near Devil's Kitchen (Figure 1). In the 2-year

Paper number 5B5915.
0148-0227/87/005B-5915$05.00

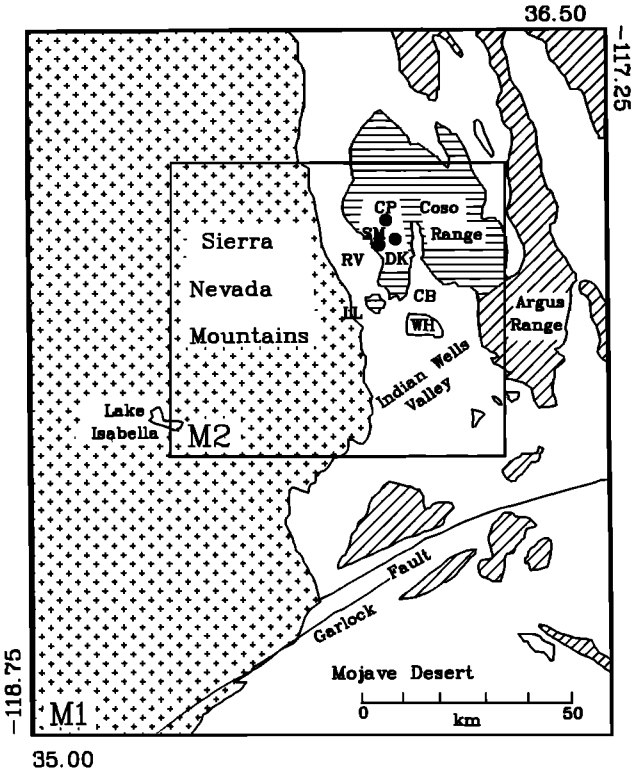

Fig. 1. Location map of study area. M1 and M2 denote areas covered by two different inversions discussed in the text. CP is Cactus Peak; SM is Sugarloaf Mountain; DK is Devil's Kitchen; CB is Coso Basin; WH is White Hills; LL is Little Lake; RV is Rose Valley. Granitic rocks of the Sierra Nevada are indicated with a crossed pattern, the Coso Range (primarily volcanics) are horizontally striped, and other bedrock is diagonally striped.

period 1975–1977, more than 4200 earthquakes occurred with $0.5 \leq m \leq 3.9$, indicating significant levels of microseismic activity [*Walter and Weaver*, 1980] (m is a coda length magnitude). Other geophysical surveys of the geothermal area have included electrical resistivity [*Jackson and O'Donnell*, 1980], aeromagnetic [*Plouff and Isherwood*, 1980], ground magnetic [*Roquemore*, 1984], and gravity [*Plouff and Isherwood*, 1980]. Results of these studies are generally equivocal regarding the location or even presence of present-day magma chambers beneath the Coso volcanic field.

Microseismic and teleseismic data are indicative of seismic anomalies near the Coso geothermal area. *Combs and Rotstein* [1976], in the first microseismicity survey of the region, reported limited observations of weak S wave shadowing from earthquakes near Cactus Peak recorded at stations to the southeast; *Roquemore and Zellmer* [1983*b*] observed possible spasmodic tremor in the same area in 1982. In a detailed seismicity study, *Walter and Weaver* [1980] noted a spoke like pattern of earthquake clusters radiating from Sugarloaf Mountain. Teleseismic data collected during that experiment were utilized by *Reasenberg et al.* [1980] in a block inversion [e.g., *Aki et al.*, 1977] for crustal velocity structure. The teleseismic residuals at Coso are smaller than at other geothermal areas such as The Geysers, Long Valley, and Yellowstone [*Oppenheimer annd Herkenhoff*, 1981; *Steeples and Iyer*, 1976; *Iyer*, 1975]. Still, stable azimuthal residual patterns enabled *Reasenberg et al.* [1980] to document a small low-velocity body in the midcrust (below 5 km) southeast of Devil's Kitchen. The absence of a gravity anomaly in the region suggests a depth of below 10 km for the anomaly [*Combs*, 1980]. This minimum depth is supported by the work of *Pavlis and Booker* [1983], based on location errors of local earthquakes at Coso. They state that velocity variations near the Coso geothermal area above 10 km are subtle, implying that any magma chamber should be below that level.

In 1981, seismic activity increased markedly in Indian Wells Valley (Figure 1) after 20 years of quiescence [*Roquemore and Zellmer*, 1983*a*]. Typically occurring in small swarms, the earthquakes have been as large as $M_L = 5.2$ [*Roquemore and Zellmer*, 1983*a*]. A Navy test track near the swarms' epicentral area underwent 3 cm of uplift between 1977 and 1978 [*Roquemore and Zellmer*, 1983*b*], indicating current surface deformation in the valley. Unfortunately, the recent extensive geophysical surveys conducted in the Coso geothermal area did not extend south to Indian Wells Valley, so relatively little is known about the area. However, early gravity and seismic refraction surveys do yield information on sediment velocities and find maximum basin depths of more than 2 km [*Healy and Press*, 1964; *Zbur*, 1963].

New seismic studies of the entire Coso region, including Indian Wells Valley, became possible after installation of several telemetered stations in the Coso region in the early 1980s. C. O. Sanders et al. (unpublished manuscript, 1986) searched for S wave shadowing across the entire region. Surprisingly, while they observed normal S waves for shallow depths in the geothermal area, they found an area of attenuated S wave propagation in Indian Wells Valley. This anomaly is extremely interesting, not only in view of the recent earthquakes and deformational activity but also because it is extremely shallow (less than 5 km).

The newly available, digital, local earthquake data also provide an opportunity to investigate the structure of Indian

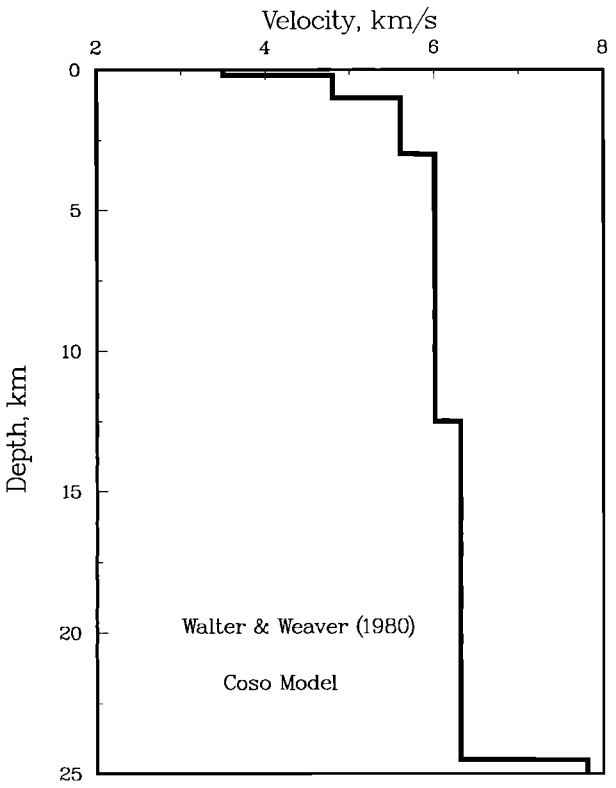

Fig. 2. Velocity model for the Coso area [*Walter and Weaver*, 1980] used in event relocation and ray tracing.

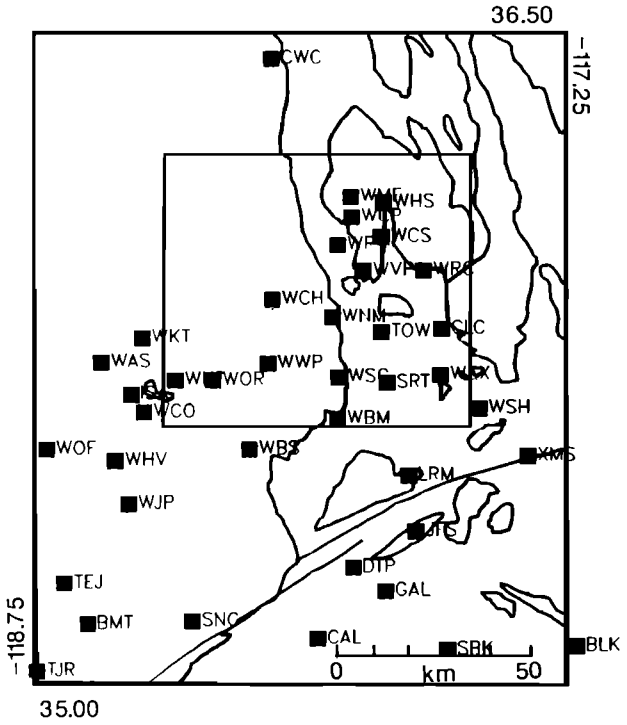

Fig. 3*a*

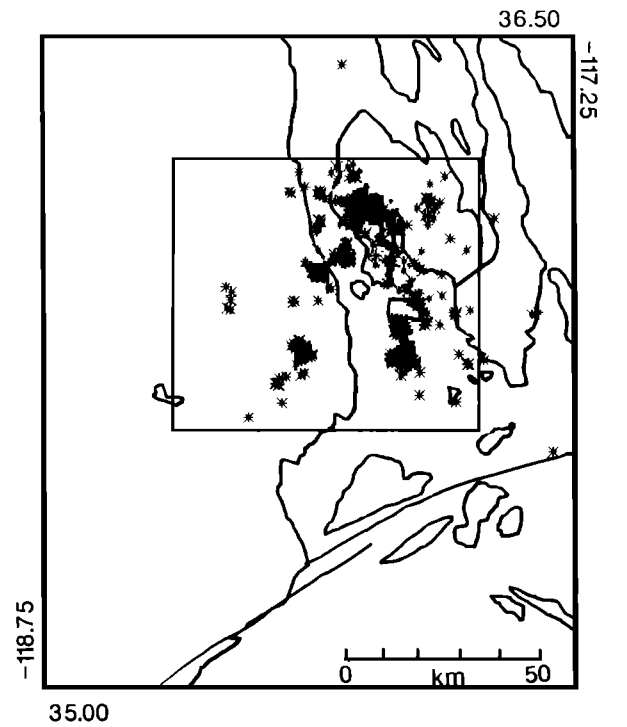

Fig. 3*b*

Fig. 3. Map view of (*a*) stations and (*b*) earthquakes used in the tomographic inversion. Small box encloses M2 model area. Outlines of the major geologic features are shown for reference. Note the clusters of seismicity.

Wells Valley and Coso using *P* wave tomography. Using local sources, we invert for three-dimensional velocity variations relative to the reference model of *Walter and Weaver* [1980]. The computational speed of the tomographic back-projection algorithm makes possible the use of extremely small blocks in the inversion, thus allowing resolution of small features. Low compressional velocities coincident with *S* wave extinction would raise the possibility of a present-day shallow magma chamber in Indian Wells Valley. Use of local data will also place more constraints on the depth to the top of the Coso teleseismic anomaly [*Reasenberg et al.*, 1980] and yield information about possible small-scale shallow extensions of that feature.

Data Set

Routinely picked travel times from events recorded at a subset of the digital Caltech–USGS southern California seismic network (SCARLET) form the data base for study of the Coso area. We selected events occurring in the 2-month period, December 1983 to January 1984, whose epicenters fall between 35.5°–36.5°N and 117.25°–118.25°W. Of the approximately 500 earthquakes, most are shallower than 8 km, but a few extend to 15 km depth, most of which are in Indian Wells Valley.

The tomographic inversion algorithm requires an accurate calculation of travel times; thus we sought the best possible locations for the events in the data set. Preliminary locations were calculated with the standard southern California velocity model [*Kanamori and Hadley*, 1975] which may not be appropriate for the Coso region. We used a standard local earthquake location program, HYPO71 (revised) [*Lee and Lahr*, 1975] and the Coso-specific velocity model of *Walter and Weaver* [1980] (Figure 2) to compute revised locations for the earthquakes in the data set. Station elevation corrections were based on the velocity of the top layer in the Walter and Weaver model and an arbitrary datum of 1000 m above sea level. Retention of all events with five or more arrival times and A, B, or C quality solutions resulted in a data set of 4036 *P* times from 429 earthquakes. The relocation procedure used both *P* and *S* times, but only *P* wave arrivals are inverted for velocity structure.

Figure 3 is a map view of the 429 new earthquake locations and the 40-station subset of SCARLET used in the relocations. The new hypocenters differ from the original locations primarily in depth and do not significantly change in horizontal position. The regional seismicity pattern is very similar to that presented by *Walter and Weaver* [1980] and resembles an inverted "V." Earthquake swarms are common in the Coso region; there are clusters to the west in the Sierra Nevada, in the geothermal area, and two distinct swarms in Indian Wells Valley. The quiescent area lies in western Indian Wells Valley and the easternmost part of the Sierra Nevada. The seismicity distribution, in combination with the station locations, provides good ray path coverage for velocity inversion below the Coso Range and is also favorable for the Indian Wells Valley region.

Inversion Method

The travel time of a seismic wave can be considered as a line integral of the slowness (inverse of velocity) field along the ray path joining the source and receiver. In general, the relationship between travel time and slowness is nonlinear; however, for small slowness perturbations and rays not near caustics, an approximate linear relation can be derived [*Aki et al.*, 1977; *Fawcett and Clayton*, 1984]. The slowness perturbations are the differences between the actual slownesses and an assumed reference slowness for the problem. The set of travel time residuals comprises the differences between the ob-

served travel times and those predicted by the reference model. The effect on the inverse problem of considering the linearized form of the relationship rather than the more accurate nonlinear form is generally a slight decrease in resolution [*Fawcett and Clayton*, 1984; *Stork and Clayton*, 1985].

By casting the problem in a discrete form, that is, dividing the three-dimensional subsurface into a set of blocks, the linearized equation can be written as

$$\Delta t_i = \sum_j l_{ij} \Delta s_j \tag{1}$$

Here Δt_i is the travel time residual of the ith ray, Δs_j is the slowness perturbation of the jth block, and l_{ij} is the ray length of the ith ray in the jth block. The summation is over all blocks in the model, so $l_{ij} \equiv 0$ for blocks not crossed by the ith ray. It is clear from the form of equation (1) that the $\{\Delta t_i\}$ is a set of linear projections of the slowness perturbations $\{\Delta s_j\}$. This means that the slowness perturbations can be reconstructed by a tomographic back-projection method.

The back-projection method used in this study is described in detail by R. P. Comer and R. W. Clayton (unpublished manuscript, 1986). The algorithm is iterative, with each iteration comprising the following calculation:

$$\Delta t_i^{(k)} = \Delta t_i^{(0)} - \sum_j l_{ij} \Delta s_j^{(k)}$$

$$u_j = \frac{\sum_i (\Delta t_i^{(k)}/L_i) l_{ij}}{\sum_i l_{ij} + \mu} \tag{2}$$

$$\Delta s_j^{(k+1)} = \Delta s_j^{(k)} + u_j$$

Here $\{\Delta s_j^{(k)}\}$ and $\{\Delta s_j^{(k+1)}\}$ refer to the kth and $(k+1)$th iterations, respectively, $\{u_j\}$ is the update, $\Delta t_i^{(k)}$ is the ith travel time residual not explained by the previous iteration, L_i is the total length of the ith ray, and μ is a damping parameter. This method is a modified version of the SIRT algorithm used in medical X ray tomography. R. P Comer and R. W. Clayton (unpublished manuscript, 1986) prove that this algorithm converges to the generalized inverse of equation (1). The damping parameter μ reduces the effect of unconstrained components of the solution. In this study μ is fixed at 100. This value appears justified in view of the noise and resolution tests discussed below. The chief advantage of the back-projection procedure over a direct solution (least squares, for example) is that it passes through the data sequentially. Consequently, very large model sizes (number of blocks) and data sets can be handled.

The application of equation (2) to deduce three-dimensional upper crustal structure in the Coso region is straightforward. The data collection process, including event relocation, insures reliable hypocenters for the events in the data set. For each source-station combination, a ray is traced through the *Walter and Weaver* [1980] velocity model (Figure 2) using a flat earth, one-dimensional homogeneous layer algorithm. The type (direct or refracted) of the first arrival is determined, and the travel time residual is calculated. Next, we follow the ray through the model, determining the ray segment length traveled in each block for each ray, thus forming the l matrix. Starting with $\Delta s_j^{(1)} \equiv 0$, we apply equation (2) until convergence is achieved.

One step in the preparation of the travel time residuals is the application of source and receiver statics. In this study the relocation of the events effectively removes the source statics from the problem (i.e., the average residual for each source is close to zero). There are, however, two approaches to the receiver static estimation. In the whole mantle studies [*Dziewonski and Anderson*, 1984; R. W. Clayton and R. P. Comer, unpublished manuscript, 1986] the receiver statics are separately estimated and removed for residuals before the inversion procedure. This is justified because the rays are nearly vertically incident at the stations. The second approach, which is used here, incorporates the statics as part of the slowness reconstruction. In this case, the top layer of the inversion will contain substantial contributions from near-surface effects. We believe this approach is necessary here because of the relatively shallow angles of emergence of the rays at the receivers.

Most of the least squares inversions for local structure have used teleseismic arrival times [e.g., *Reasenberg et al.*, 1980]. Teleseismic rays arrive at steep incidence angles, providing good lateral coverage, but velocity anomalies may be smeared out in depth because of vertical coupling between blocks. Use of local phases helps to more precisely determine depth extent, since most rays are composed of several segments with differing incidence angles. The depth to the bottom of the region's seismogenic zone limits the depth resolution of an experiment using local sources, however, as does the array aperture. The event locations also limit the model azimuthal coverage. The ideal crustal imaging experiment would include a combination of local, regional, and teleseismic data to insure a maximum sweep of incidence angles.

The Coso data set, which includes earthquakes to depths of more than 15 km, should provide a reliable image of upper crustal velocities to depths of about 8 km with good azimuthal coverage. In general, the center of the model spaces are most reliable because of the higher number of crossing rays each cell receives. The results of inversion of the 4036-ray data set with two models with differing block sizes are described in the next section.

INVERSION RESULTS

We present two models of the lateral velocity variations in the Coso region derived from the same data but with different areal extents and block sizes. The area of model M1 is represented in Figure 1 as the outer boundary; it covers 22,275 km^2 with 4455 blocks, 891 in each of five layers. Each cell has surface dimensions of 5 × 5 km, and the five layers in depth are of varying thickness, from 2 to 10 km. Model M2 (see the inner rectangle in Figure 1 for location) covers a much smaller area of only 5600 km^2 with 11,200 blocks, 1400 in each of eight layers. With surface dimensions of only 2 × 2 km and significantly thinner layer thicknesses, M2 should provide more resolution of fine features than the regional model M1.

The number of rays crossing a model block is an important parameter in assessing the inversion results. Figure 4 graphically displays selected layers of the "hit count" matrices for both M1 and M2. Figure 4*a* shows the hit counts for M1 with the outline of the M2 model superimposed for scaling purposes. Many cells are not crossed by any rays, and it is easy to see that the ray coverage speads out with increasing depth. The smaller block size of M2 is reflected in the hit count map of Figure 4*b*. Individual stations are detectable for layer 1 (0–1 km) and "streaking" due to prominent ray paths is visible for several other layers. Layers 3 and 4 have the most uniform ray distribution for M2.

Figure 5 presents the inversion results for M1, the regional model. The block size of 5 × 5 km is the same as that of the

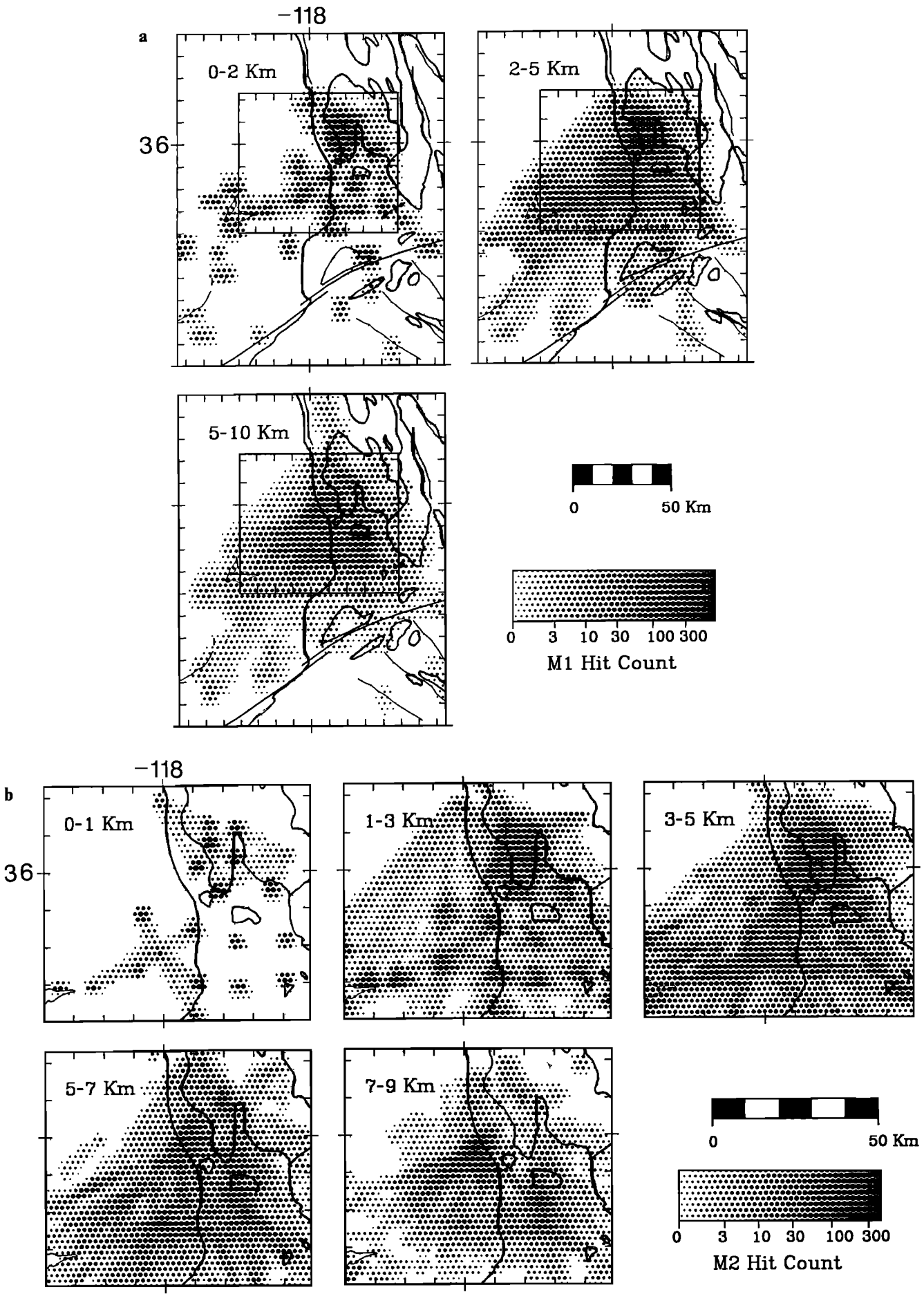

Fig. 4. Hit count maps for models M1 and M2. The size of each dot is proportional to the number of rays hitting each block, with the largest dots representing 100 or more hits. Tick marks are separated by 0.1°. (*a*) M1. Only the top three layers are shown M2 outline appears for reference. (*b*) The top five layers of M2. Clusters in layer 1 represent individual stations Ray coverage is best for the 3–5 km and 5–7 km layers.

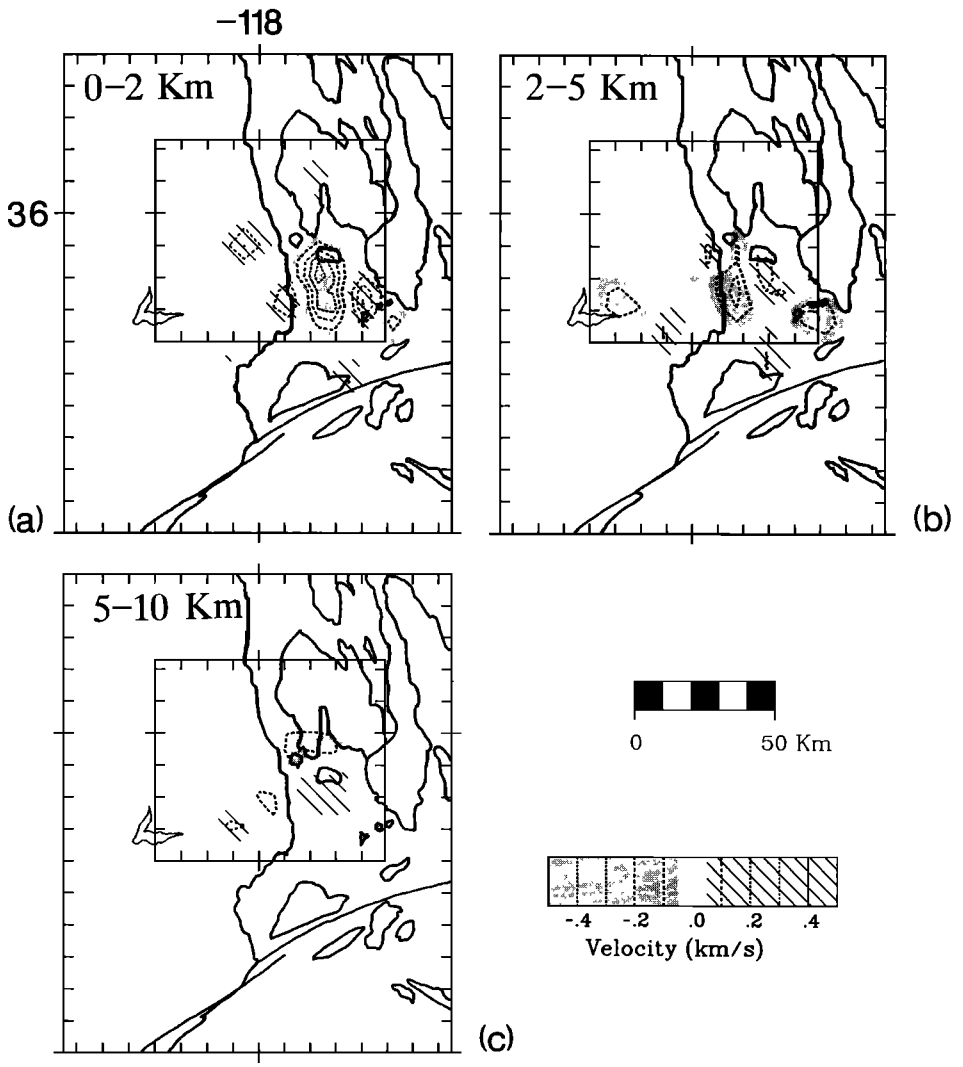

Fig. 5. Tomographic inversion results for the top three layers of M1. Outlines from Figure 1 are shown for location as well as a box enclosing M2. Slowness values for each cell are weighted using the number of ray hits per cell in order to emphasize well-resolved areas. The contour interval is 0.1 km/s. (*a*) Layer 1, 0–2 km depth. Note the intense low velocities in IWV and relatively fast areas in the Sierra Nevada and Argus ranges. (*b*) Layer 2, 2–5 km depth. Western IWV has low velocities. Coso Range is neutral. (*c*) Layer 3, 5–10 km depth. IWV is now neutral to fast, while the southern Coso volcanic field is slow.

Reasenberg et al. [1980] Coso teleseismic least squares block inversion, but M1 covers a much larger area. In each panel the inner square again marks the area covered by model M2. In order to emphasize well-sampled features the slowness results are weighted according to a ramp function depending on the number of hits per cell; a cell with 100 hits receives a weight of 1, decreasing linearly to 0 weight for fewer than two hits. The slowness matrix is slightly smoothed before contouring. Slow areas are shaded, fast areas striped, and the contour interval is 0.1 km/s.

The top layer represents depths of 0–2 km (Figure 5*a*) and contains information primarily on receiver statics. Indian Wells Valley (IWV) has negative velocity anomalies (low velocities) in this layer, as would be expected from the deep pile of sediments in the basin (to 2 km; see *Healy and Press* [1964]). The Coso and Argus ranges are neutral to relatively fast, as is most of the Sierra Nevada. These anomalies correlate well with surface geology, suggesting that the surface statics migrate into the top layer during the inversion process.

The second layer of M1 covers the depth range of 2–5 km. The dominant feature in Figure 5*b* is a concentrated low-velocity region in Indian Wells Valley, now shifted west of its surface expression (Figure 5*a*). The IWV anomaly reaches westward into the Sierra Nevada at about 35.8°N and continues northward to the White Hills. Smaller low-velocity anomalies appear to the west (35.75°N, 118.30°W) and east (35.7°N, 117.50°W) but are not strong as the IWV anomaly, which reaches a maximum velocity contrast of more than 10% (−0.59 km/s). Rose Valley and the Coso geothermal areas are neutral at these depths, while the alluvial Coso Basin (see Figure 1 for location) is faster than the reference model from 2 to 5 km depth.

The velocity variations in layer 3 (Figure 5*c*) are generally less intense than those for the shallower layers. The portion of Indian Wells Valley that is slow from 2 to 5 km depth is now slightly faster than the 6.0 km/s reference velocity for this depth range. An area of reduced velocity just west of the Sierran front at 35.8°N could be a continuation of the IWV anomaly to greater depth, indicating a possible westward dip for the anomaly. In the Coso volcanic region a fairly broad

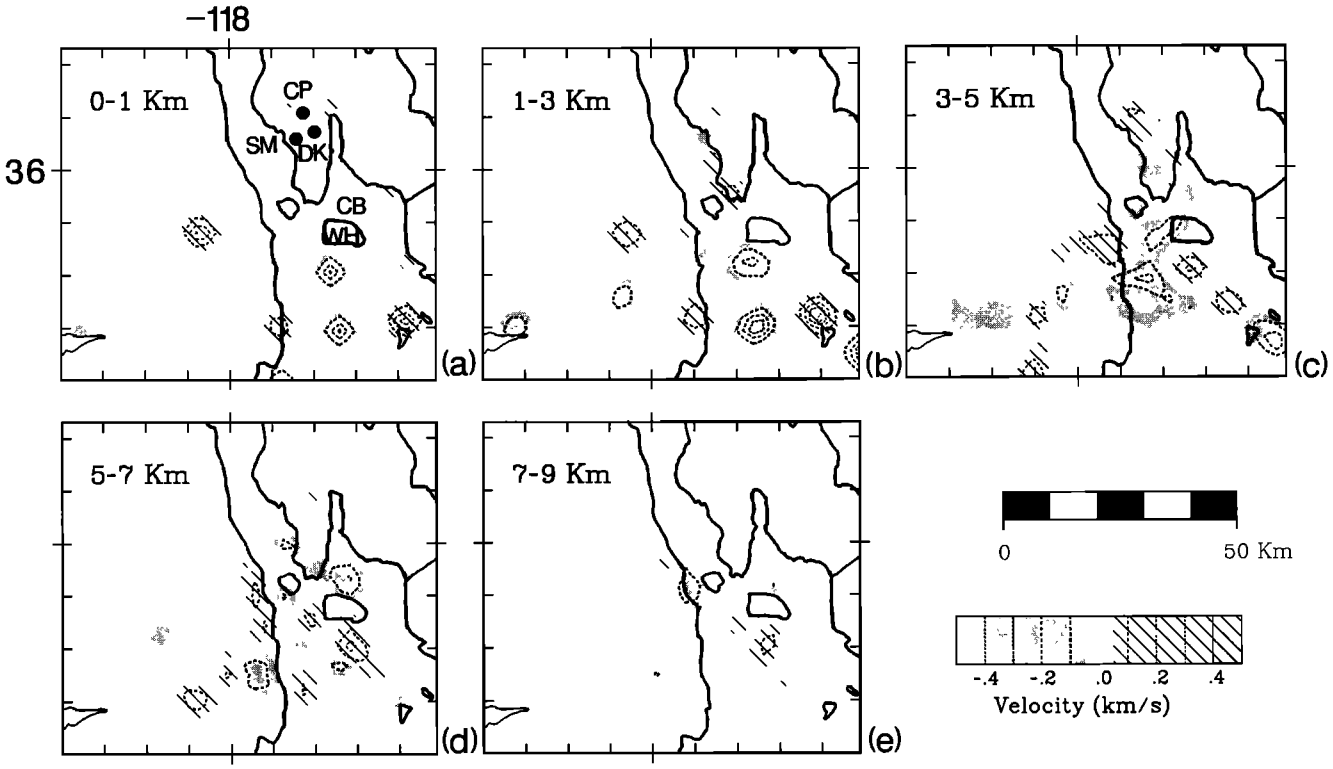

Fig. 6. Tomographic inversion results for the top five layers of M2. See Figure 5 for scaling scheme and location relative to M1. (*a*) Layer 1, 0–1 km. Letters indicate place names found in Figure 1. Smaller block size (2 × 2 km) of M2 provides better resolution; individual station anomalies are visible. Stations in the western Indian Wells Valley are particularly slow. (*b*) Layer 2, 1–3 km. Station surface statics continue into this layer, slightly spread out. (*c*) Layer 3, 3–5 km. IWV contains two intense low-velocity regions at these depths at the west and north ends of the valley. There are also low velocities near Cactus Peak and the southern Coso Range. (*d*) Layer 4, 5–7 km. Low velocities are found under the Coso Basin, extending to the northwest toward the volcanic field. (*e*) Layer 5, 7–9 km. The IWV anomaly has disappeared by these depths. While the area beneath the volcanics appears neutral, ray coverage is not as good for this layer, so deeper anomalies may not be resolved.

low-velocity anomaly reaches a maximum contrast of about 8% (−0.48 km/s) southeast of Devil's Kitchen. After the smoothing is applied, this feature covers 20 km in the E-W dimension and so extends beyond the volcanics' surface expression. We note that due to the fairly large block size of M1, images of small velocity features may be blurred in this model. Because most earthquakes in the Coso area occur above 10 km depth, we limit our inversion interpretation to the top three layers of M1.

The regional model M1 provides a broad view of the velocity anomalies with fairly coarse resolution; we now use the higher-resolution model M2 to "zoom in" on a smaller portion of the Coso region in more detail. We expect the main features of M2 to be equivalent to those inside the boxed area of Figure 5 but more sharply focused.

The two top layers of M2 (Figures 6*a* and 6*b*) represent depths of 0–1 and 1–3 km, respectively. Individual station statics are easily seen in Figure 6*a*, dominated by slow velocities for stations in the western Indian Wells Valley, and fast values for stations to the east and west. The second layer (Figure 6*b*) is primarily an extension of layer 1, with the station static anomalies spreading out with depth.

The velocity variations change substantially in layer 3 of M2 (Figure 6*c*), extending from 3 to 5 km in depth. An area of low velocity hugs the Sierra Nevada frontal fault line from 35.8°N to 36°N, with more intensely slow areas centered southwest of station TOW and west of the White Hills. This low-velocity area is coincident with that of layer 2 in M1 but shows more detail. The northern of the two IWV anomalies actually lies just south of the Coso volcanics. The other anomaly occupies the western side of IWV. The Coso range itself is nearly neutral at these depths, except for two very small, low-velocity anomalies located directly below Cactus Peak and south of Sugarloaf Mountain. These anomalies are not resolved with the M1 inversion due to their small sizes. The eastern part of IWV is relatively fast at these depths.

In the 5–7 km depth range (Figure 6*d*) the IWV anomaly is weakened; small areas of low velocity remain to the west and east of the 3–5 km anomaly location. There are slow features beneath the Coso field in this depth range centered just west of Sugarloaf mountain and also 10 km southeast of Devil's Kitchen. The latter anomaly is probably related to the *Reasenberg et al.* [1980] teleseismic low-velocity body, which is centered in the same area. The fast anomaly in eastern Indian Wells Valley, seen in layer 3, remains stable in layer 4.

The hit count map for M2 (Figure 4*b*) reveals that at depths corresponding to layer 5 (7–9 km), ray coverage in the Coso geothermal area is poor, so we cannot follow the layer 4 anomalies any deeper with these data. There is an interesting area of low velocity near Little Lake in the Sierra Nevada at these depths, and there is a hint of an extension of the southern Coso anomaly described above (for layer 4) into this depth range. Indian Wells Valley, still with reasonable ray coverage, is primarily neutral from 7 to 9 km.

The results of the tomographic inversion are encouraging; the surface layers reflect local geology, and at greater depths

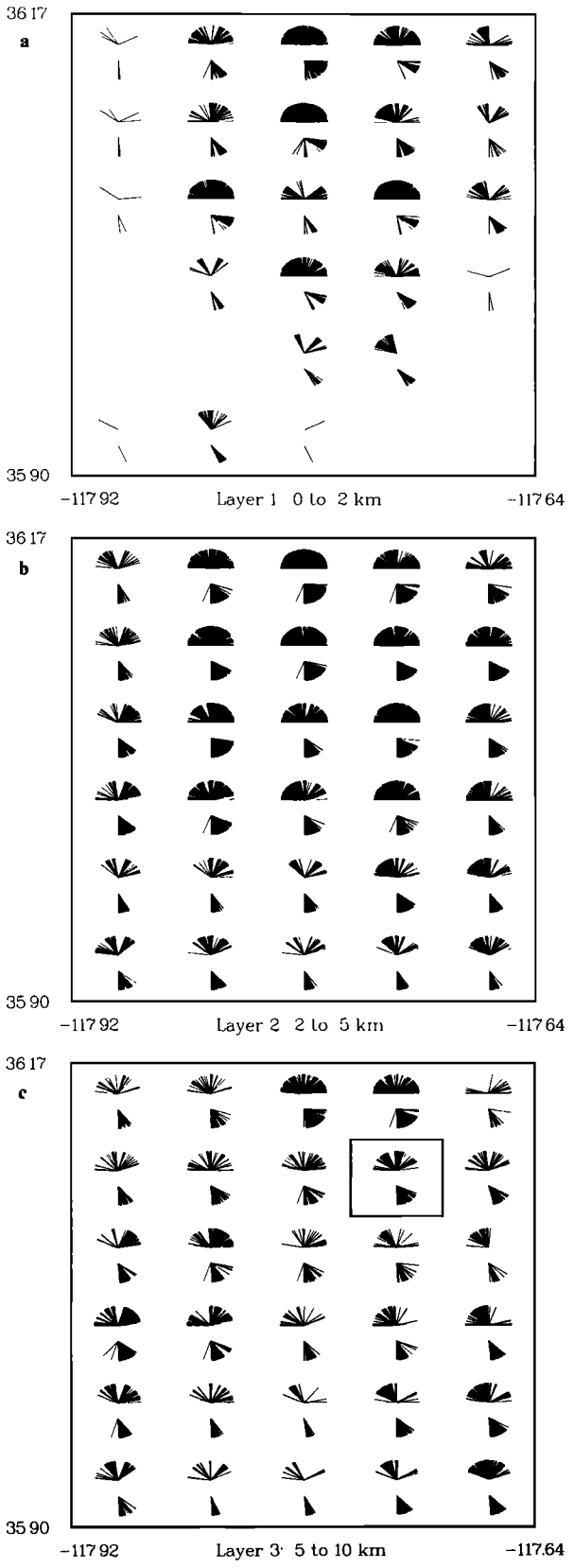

Fig. 7. Azimuth and incidence angle distribution for a portion of model M1 for a range of depths. Shown is a suite of blocks in the rhyolite dome area for layers 1–3. The azimuth coverage is seen in the top half of each block; a complete semicircle indicates perfect azimuthal coverage. The incidence angle coverage occupies the lower half of each block, with downgoing rays appearing in the left half of the semicircle, upgoing rays in the right half, and horizontal rays in the center. Both layers 2 and 3 have excellent ray coverage. A heavy line marks the block in layer 3 used in the single-cell resolution experiment.

the principal seismic anomalies correlate well with those found with other methods.

Model Stability and Resolution

The issues of model resolution and stability are important in assessing the reliability of any inversion result. Because we do not automatically compute a resolution matrix with the back-projection inversion scheme, we consider both the number of hits per block and the predominant vector ray directions in each block in evaluating the inverted slowness values. If a cell is hit only a few times, any individual slowness parcels assigned to that cell that are in error have a much larger effect than if many rays ($\geq$ 100) hit each cell. Thus blocks with large "hit counts" are more likely to represent the true character of the slowness in those blocks, since random errors more probably cancel out. If a cell is hit many times but each ray is coming from the same direction, then the resolution may also be poor, since that cell is strongly coupled to those surrounding it.

By inspecting the distribution of ray azimuths and incidence angles for each cell, we can qualitatively assess a particular block's reliability in the inversion result. Figure 7 displays the azimuth/incidence angle coverage for a portion of model M1 at several different depth levels. These ray patterns are constant for each model; M2 has different distribution characteristics. For both azimuth and incidence angle, a solid half-circle indicates perfect coverage, since reciprocity implies the filling of the other half of the circle. The coverage for both parameters is excellent for the interior portion of M1, especially in layers 2 and 3 (2–10 km). Coverage degrades severely in the Coso volcanic region below 10 km for M1. Ray incidence is more nearly vertical for layer 1 (0–2 km), as expected, while poorly sampled cells are hit by mostly horizontally traveling rays in the layers below.

We can assess the ray set's sensitivity to random noise, such as would be generated by timing errors, by performing a numerical experiment. The Coso travel time residual data most closely resemble a double exponential distribution (Figure 8) with a median of 0.001 s and an L_1 deviation of 0.0974. We generated two sets of 4036 random numbers with the same statistical characteristics and replaced the data time residuals with the synthetic data, or noise. Inversion of one set of the random numbers using the actual data ray paths and model M1 produces the result shown in Figure 9. Although the variance of the random numbers is equivalent to that of the data, the maximum slowness anomaly observed is only half of the data value. The inversion, even after 50 iterations, explains only 4% of the random time residuals. The large slowness values concentrate in areas of poor ray coverage, such as the edges of the sampled areas. These characteristics differ significantly from those of real data inversions, indicating that random noise does not dominate the data set. Replacing the entire data set with random noise is a worst case test (R. P. Comer and R. W. Clayton, unpublished manuscript, 1986). The true expectation of the noise component of the solution would be the average of many such simulations.

The ambient noise level in midmodel is 5–10% of the data maximum variation value. In order to be considered significant, data anomalies must be more than 10% of the maximum value for the inversion.

Numerical tests with synthetic velocity anomalies and the actual ray configuration assist in determination of the resolving power of the data in key localities. Two such experiments were performed: one with a single-cell, large contrast anomaly, and a second incorporating a model of the region's surface

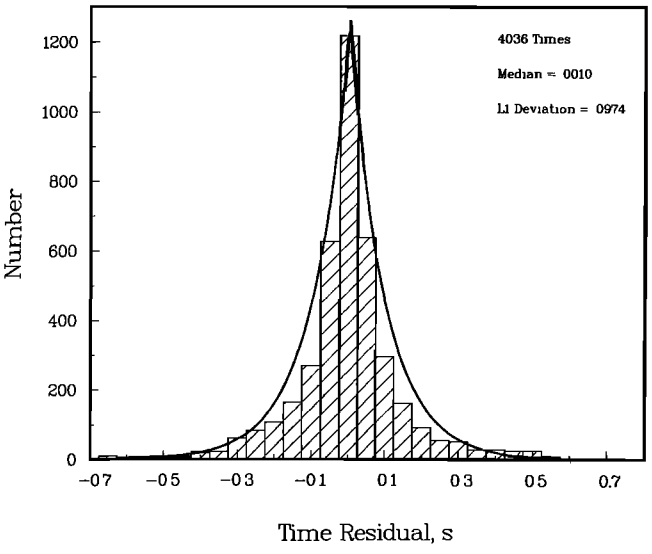

Fig. 8. Distribution of Coso travel time residuals for 4036 rays in 0.05-s windows. The distribution has a median of 0.001 s and an L_1 deviation of 0.0974. The double exponential distribution for these values is superimposed on the residual histogram.

geology in order to determine its effect on perceived velocity anomalies at greater depth. For these experiments, all travel time residuals are set equal to zero except when a ray travels through a block with a predetermined synthetic velocity anomaly.

Figure 10 presents portions of the top three layers for a resolution test consisting of a 20% velocity reduction in one cell below the Coso volcanic field in layer 3 (5–10 km) of M1. From the azimuth/incidence angle distribution (see Figure 7) we note that this area has excellent ray coverage, so we expect near-optimal model resolution for the region. The synthetic inversion results are excellent: We achieve a 96.8% variance reduction, with 99% of the anomaly placed into the correct block; there is no lateral or vertical streaking in this case.

We examined the effects of surficial features on our inversion results at depth by using a model incorporating the slow sediments of IWV and Rose Valley and the relatively fast granites of the Sierra batholith. Using M2, we assigned a 30% velocity decrease for IWV in layer 1 and 10% in layer 2, a 10% decrease for Rose Valley, and a 20% increase for the Sierra Nevada mountains. Figure 11 shows the results for the top five layers; compare to the data (Figure 6). We observe the maximum delay in IWV sediments, as expected, and fast

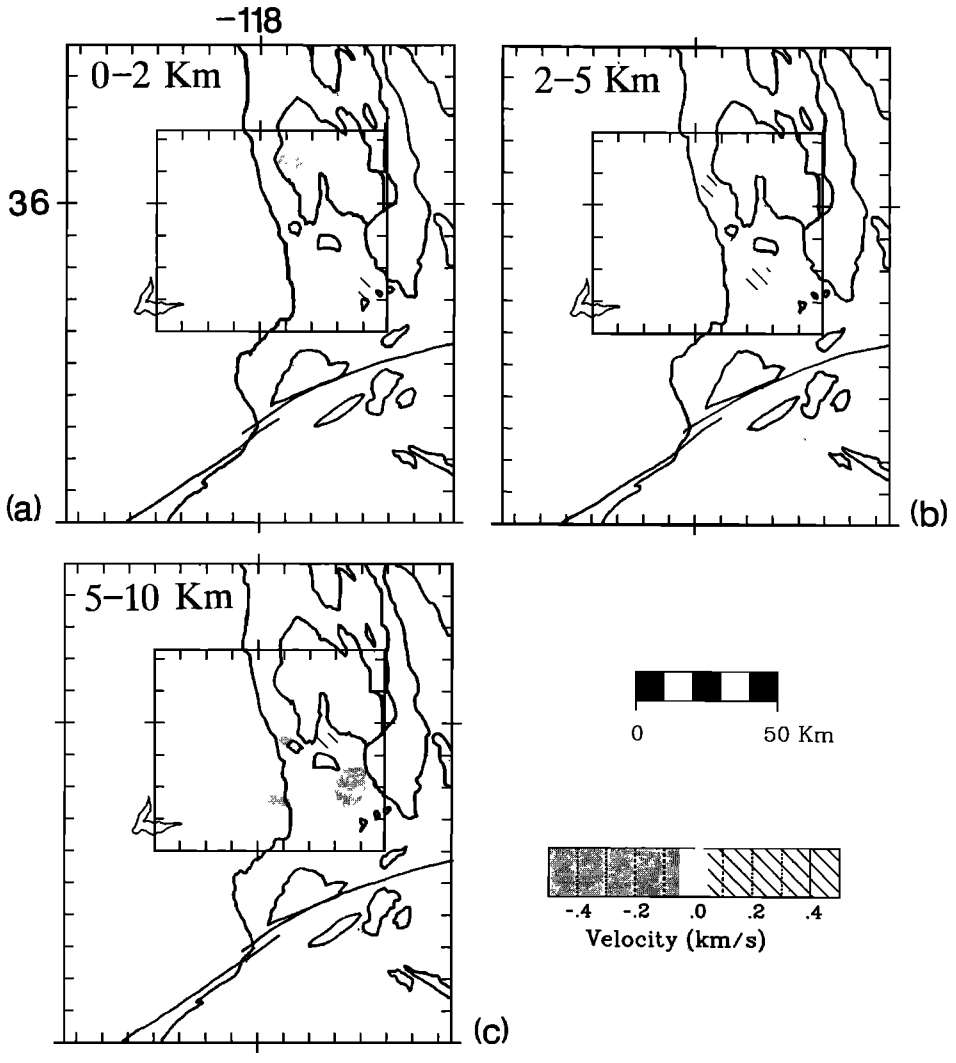

Fig. 9. Noise test inversion results for the top three layers of M1. The format and scale are the same as in Figure 5. Random numbers with a double exponential distribution with the same median and L_1 deviation as the data replaced the travel time data in this inversion Note the low magnitude of the velocity changes.

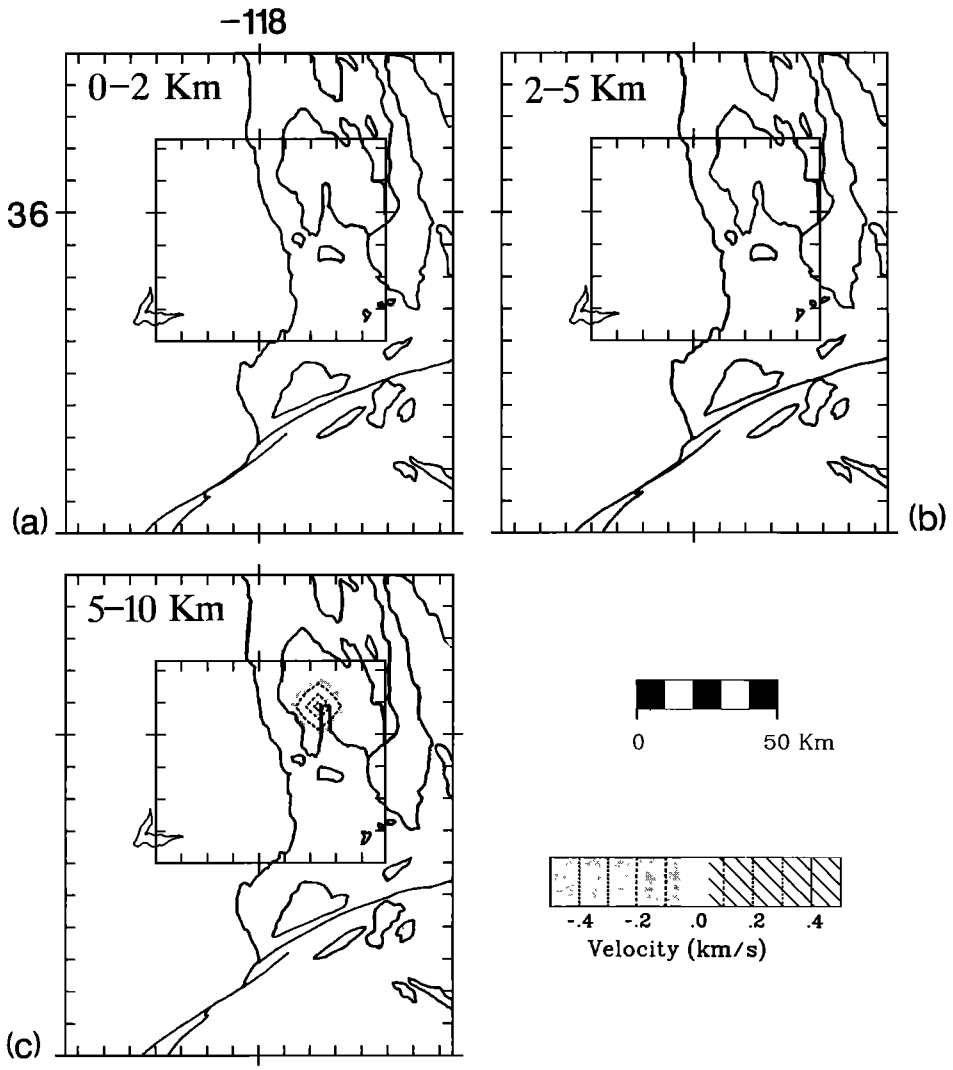

Fig. 10. Resolution test inversion results for a single-cell synthetic velocity anomaly placed in layer 3 (5–10 km) of M1. The azimuth and incidence angle coverage for that cell is indicated in Figure 7. The format and scale are as in Figure 5. The reconstruction of the synthetic anomaly is excellent in both location and amplitude.

values to the west of the Sierran front in layer 1. Layer 2 matches the data quite well, particularly in IWV. For layer 3 (3–5 km) we observe a streaking of 10–20% of the data maximum into some areas which also appear slow in the data inversion. The data values for the same location, however, are 30–50% of the data maximum, indicating that while the sediments do produce apparent low velocities at this location, the amplitudes are less than half of the observed values. More low-velocity material from 3 to 5 km is required to match the travel time data. Addition of a 6% velocity decrease below western IWV in layer 3 increases the synthetic anomaly to observed levels. We obtained a similar result for M1. The resolution tests thus indicate that our ray set has the resolving power to determine real low-velocity anomalies at depth below both Indian Wells Valley and the Coso volcanic field.

Discussion

The application of a tomographic back-projection technique to local earthquake travel times in the Coso region, California, has yielded a detailed three-dimensional picture of velocity variations over a large area. Utilizing only elevation corrections, we have recovered surface layer statics which correlate closely to surface geology. The inversion also reveals velocity anomalies at depths ranging from 2 to 10 km which may be related to the tectonic activity of the Coso region. The resolution and stability of the inversion has been investigated using numerical experiments with both random number distributions (variance) and synthetic velocity anomalies (resolution). The noise tests demonstrate that the Coso data contain significant information about lateral velocity variations. The ambient noise level due to timing errors is 5–10% of the maximum slowness variation. Tests with synthetic anomalies show that deep anomalies beneath both the Coso volcanic field and Indian Wells Valley are generally well-resolved. Synthetic anomalies placed in the 1–3 km depth range (M2) are partially imaged in the surface layers; the converse is also true. While surficial sediment piles do "leak" some low velocities into the 3–5 km depth range, the observed velocity change in IWV is 3 times as large as the sediment-produced effect. Velocity variations in the subsurface layers in cells which have a large hit count, good azimuthal and incidence angle coverage are reliable and well-resolved.

Perhaps the most interesting result of the inversion is the area of low P wave velocity in the depth range 3–5 km beneath western Indian Wells Valley and the White Hills. Indian Wells Valley is one of a series of range front basins on the east side of the Sierra Nevada [*Healy and Press*, 1964]. As much as 2 km of Cenozoic sediments reside in the basin [*Zbur*, 1963;

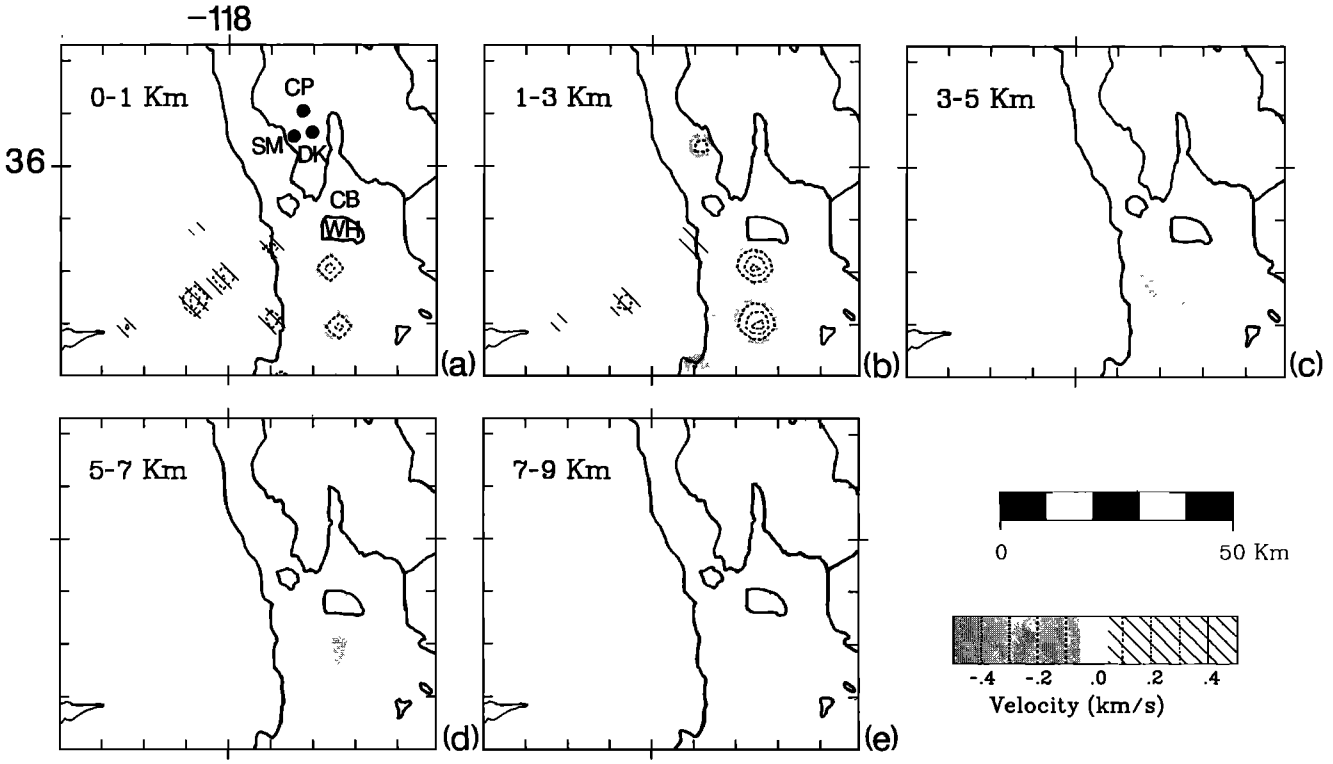

Fig. 11. Resolution test inversion results for multicell synthetic velocity anomalies representing the surface geology for M2. The top five layers are shown. The format and scale are as in Figure 6. This experiment tests the effects of the surfical velocity variations (such as those associated with sediment piles) on inferred deeper structure; compare to Figure 6, the data inversion results. The top two layers are very similar in both figures, indicating that the sediment model is realistic. Below 3 km, the Indian Wells Valley sediments contribute little to the inversion results (see above). The dominant features of the data inversion at depth, therefore, are not caused by poor ray sampling but represent real velocity changes.

Healy and Press, 1964] along its western side. Gravity modeling and seismic refraction experiments [*Zbur*, 1963] suggst faulting within Indian Wells Valley, and strike-slip and graben structures are observed at the surface [*Roquemore*, 1981]. At the northern end of Indian Wells Valley are the White Hills, an anticline formed of Quaternary sedimentary rocks with basalt flows to the west.

Inversions with both the M1 and M2 models show a strong low-velocity region in western IWV, stretching north to the White Hills. Although there are no surficial volcanics in IWV, it is the locus of contemporary deformation and earthquake swarms [*Roquemore and Zellmer*, 1983*a*]. Further, *Zbur* [1963] attributed a high-velocity arrival on a refraction profile, which correlated with an aeromagnetic high, to a volcanic layer embedded within the Cenozoic sediments at a shallow level. C. O. Sanders et al. (unpublished manuscript, 1986) observe *S* wave shadowing in the western portion of the valley; their anomaly correlates somewhat with the southern *P* wave low-velocity region (Figure 12). If the Coso region is a local spreading center, as *Weaver and Hill* [1979] suggest, then continued magmatic activity is consistent with the observed data. The detection of low *P* wave velocities is not sufficient to completely characterize the nature of the anomaly. A known geothermal system near Devil's Kitchen does not produce any *P* wave anomaly in the same inversion; the coincidence of the shear wave depletion anomaly and the low *P* wave velocities makes partial melting a possible cause for the seismic anomalies. The lack of other detailed geophysical data for Indian Wells Valley maker further interpretation problematic.

For model M1, which can resolve features no smaller than 5 km, the tomographic inversion is featureless above 5 km depth in the Coso volcanic region. This is not too surprising, since we use a reference model specifically designed for the area [*Walter and Weaver*, 1980] and since *Pavlis and Booker* [1983] believe, based on microearthquake location residuals,

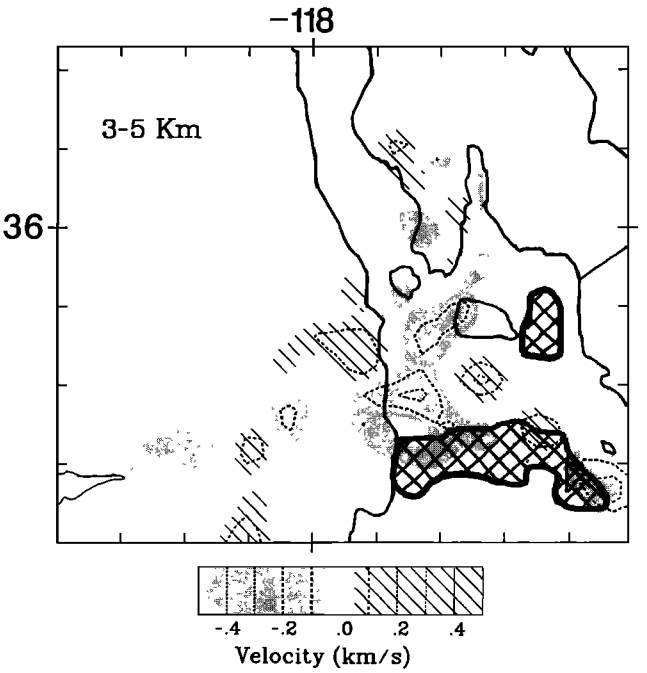

Fig. 12. Map view comparing location of IWV anomaly and C. O. Sanders et al. (unpublished manuscript, 1986) *S* wave anomaly at the 3–5 km depth level (hatched). The two anomalies overlap in the southern portion of the valley but are not entirely coincident.

that any velocity variations above 10 km depth at Coso are extremely subtle. The geologic and geophysical data for the Coso volcanic field, however, are anything but uniform. *Combs* [1980] documents an area of extremely high heat flow near Devil's Kitchen, and *Young and Ward* [1980] discovered areas of high seismic wave attenuation in the same area, probably due to the geothermal activity. The gravity and aeromagnetic patterns [*Plouff and Isherwood*, 1980] are complex but may be more related to regional tectonics than to local volcanic activity. The available background information suggests a relatively deep magma body at Coso. *Young and Ward*'s [1980] attenuation results find low Q below 12 km depth, and the teleseismic inversion of *Reasenberg et al.* [1980] places the low-velocity body in midcrust, although the upper bound is as shallow as 5 km. Geologic arguments [*Bacon et al.*, 1980; *Bacon*, 1985] also suggest that the main magma body is deep.

Back-projection of the local earthquake data results in an area of low velocity, primarily south of the volcanic field, between 5 and 10 km depth. The block with the maximum slowness anomaly is located beneath the Coso Basin, about 10 km southeast of Devil's Kitchen, in an area not well-covered by previous seismic experiments. The unsmoothed data show a northwest-southeast trend of low velocity, averaging 7% slow (−0.42 km/s), from just southwest of Sugarloaf Mountain to the Coso Basin. This area is partially coincident with the Reasenberg et al. teleseismic anomaly and may be associated with it. The depth to the top of the teleseismic anomaly is uncertain and may be as great at 10 km, since the depth resolution of inversions of steeply incident teleseismic P waves is fairly poor. Few rays from our local earthquake data set penetrate deeper than 10 km beneath the Coso Range, so our tomographic inversion would probably not image an anomaly at 10 km or greater depth beneath Devil's Kitchen. Thus, if the Reasenberg et al. anomaly is fairly deep, the local earthquake data cannot resolve it, and it will not appear in the tomographic inversion results. The Reasenberg et al. teleseismic data, on the other hand, do not cover the Coso Basin area in the midcrustal depth range, so the Coso Basin anomaly as seen in the tomographic results would not appear in the teleseismic inversion. The study areas of *Pavlis and Booker* [1983] and *Young and Ward* [1980] also lie primarily to the north of the Coso Basin anomaly, where we do not observe large velocity variations at midcrustal depths.

The present-day surface heat flow anomaly [*Combs*, 1980] and the geothermal activity do not coincide with any documented, shallow P wave velocity anomalies. The hydrothermal system and the high heat flow may well be due to the same source, which could be offset from the larger, deeper magma body.

With the more finely gridded model, M2, we can attempt to resolve features as small as 2 km across. An anomaly covering parts of only two cells appears in the 3–5 km layer for M2 below Cactus Peak, a rhyolite dome north of Sugarloaf Mountain. *Bacon et al.* [1981] place Cactus Peak in the youngest group of Coso rhyolite domes, and *Roquemore and Zellmer* [1983*b*] observed possible spasmodic tremor there in 1982. This anomaly continues, still very small, into the 5–7 km layer; limited ray coverage precludes following it any deeper. In layer 4 of M2 (5–7 km) we observe other small slow anomalies just south and west of Sugarloaf, beneath it, and also below the Coso Basin. These features are in similar locations to those described above for M1.

The bulk of any P wave low-velocity anomaly in the Coso volcanic region may well reside below 10 km. We cannot resolve such a body with our data due to insufficent ray coverage at those depths. The anomalies described above could be small, shallow projections of the major magma chamber. With small dimensions and density contrasts, such bodies might go undetected in gravity surveys. Addition of regional and teleseismic data to the local times used in this study would better define the deep crustal structure of the region while retaining good resolution of shallow features. It is clear that the Coso region is tectonically active because of its high heat flow, geothermal system, high seismicity rate, and comtemporary geodetic deformation. The tomographic inversion indicates that the deep magma chamber may have shallow extensions just south of the present Coso volcanic field, primarily in the 5–10 km depth range and perhaps to 3 km below Cactus Peak. The Indian Wells Valley region, a few kilometers farther south, contains shallow areas of low P wave velocity which also attenuate S waves (C. O. Sanders et al., unpublished manuscript, 1986), and which has abundant seismic acitivity up to the $M_L = 5$ level [*Roquemore and Zellmer*, 1983*a*]. The IWV seismic anomalies weaken or disappear below 5 km depth. These features could be related to current magmatic processes in the subsurface; more geophysical data are needed to understand better the details of the tectonic activity occurring in Indian Wells Valley.

Acknowledgments. This study was supported by the U.S. Department of Energy under contract DE-AC04-76DP00789 and by the U.S. Geological Survey under contract 14-08-0001-G1171. Some of the graphics and computational facilities were provided by the W. M. Keck Foundation. We thank Chris Sanders and Hiroo Kanamori for their close cooperation during this study and their critical reviews of the manuscript. The assistance of Carl Johnson and Doug Given of the USGS Pasadena office was invaluable in obtaining the earthquake data. Greg Elbring provided computer graphics expertise. Contribution 4251, Division of Geological and Planetary Sciences, California Institute of Technology, Pasadena, California.

REFERENCES

Aki, K., A. Christofferson, and E. Husebye, Determination of the three-dimensional seismic structure of the lithosphere, *J. Geophys. Res.*, *82*, 277–296, 1977.

Austin, C. F., W. H. Austin, Jr., and G. W. Leonard, Geothermal science and technology—A national program, *Pap. 45-029-72*, 95 pp., U.S. Nav. Weapons Cent. Tech. Serv., China Lake, Calif., 1971.

Bacon, C. R., Time-predictable bimodal vocanism in the Coso Range, California, *Geology*, *10*, 65–69, 1982.

Bacon, C. R., Implications of silicic vent patterns for the presence of large crustal magma chambers, *J. Geophys. Res.*, *90*, 11,243–11,252, 1985.

Bacon, C. R., W. A. Duffield, and K. Nakamura, Distribution of quaternary rhyolite domes of the Coso Range, California: Implications for extent of the geothermal anomaly, *J. Geophys. Res.*, *85*, 2425–2433, 1980.

Bacon, C. R., R. Macdonald, R. L. Smith, and P. A. Baedecker, Pleistocene high-silica rhyolites of the Coso Volcanic Field, Inyo County, California, *J. Geophys. Res.*, *86*, 10,223–10,241, 1981.

Combs, J., Heat flow in the Coso Geothermal Area, Inyo County, California, *J. Geophys. Res.*, *85*, 2411–2424, 1980.

Combs, J., and Y. Rotstein, Microearthquake studies at the Coso Geothermal Area, China Lake, California, in *Proceedings of the 2nd United Nations Symposium on the Development and Use of Geothermal Resources*, vol. 2, pp. 909–916, U.S. Government Printing Office, Washington, D. C., 1976.

Duffield, W. A., Late Cenozoic ring faulting and volcanism in the Coso Range area of California, *Geology*, *3*, 335–338, 1975.

Duffield, W. A., and C. R. Bacon, Geologic map of the Coso volcanic field and adjacent areas, Inyo County, California, *U.S. Geol. Surv. Misc. Invest. Ser. Map, I-1200*, 1981.

Duffield, W. A., C. R. Bacon, and G. B. Dalrymple, Late Cenozoic volcanism, geochronology and structure of the Coso Range, Inyo County, California, *J. Geophys. Res.*, *85*, 2381–2404, 1980.

Dziewonski, A. M., and D. L. Anderson, Seismic tomography of the earth's interior, *Am. Sci.*, *72*, 483–494, 1984.

Fawcett, J. A., and R. W. Clayton, Tomographic reconstruction of velocity anomalies, *Bull. Seismol. Soc. Am.*, *74*, 2201–2219, 1984.

Healy, J., and F. Press, Geophysical studies of basin structure along the eastern front of the Sierra Nevada, California, *Geophysics*, *29*, 337–359, 1964.

Hearn, T. M., and R. W. Clayton, Lateral velocity variations in southern California, I, Results for the upper crust from *Pg*-waves, *Bull. Seismol. Soc. Am.*, *76*, 495–509, 1986*a*.

Hearn, T. M., and R. W. Clayton, Lateral velocity variations in southern California, II, Results for the lower crust from *Pn*-waves, *Bull. Seismol. Soc. Am.*, *76*, 511–520, 1986*b*.

Humphreys, E. D., R. W. Clayton, and B. H. Hager, A tomographic image of mantle structure beneath southern California, *Geophys. Res. Lett.*, *11*, 625–627, 1984.

Iyer, H. M., Anomalous delays of teleseismic *P* waves in Yellowstone National Park, *Nature*, *253*, 425–427, 1975.

Jackson, D. B., and J. E. O'Donnell, Reconnaissance electrical surveys in the Coso Range, California, *J. Geophys. Res.*, *85*, 2502–2516, 1980.

Kanamori, H., and D. Hadley, Crustal structure and temporal velocity change in southern California, *Pure Appl. Geophys. 113*, 257–280, 1975.

Kissling, E., W. L. Ellsworth, and R. S. Cockerham, Three-dimensional structure of the Long Valley caldera, California, region by geotomography, Proceedings of Workship XIX, Active Tectonic and Magmatic Processes Beneath Long Valley, Caldera, Eastern California, vol. I., *U.S. Geol. Surv. Open File Rep.*, *84-939*, 188–220, 1984.

Lanphere, M. A., G. B. Dalrymple, and R. L. Smith, K-Ar ages of Pleistocene rhyolitic volcanism in the Coso Range, California, *Geology*, *3*, 339–341, 1975.

Lee, W. H. K., and J. C. Lahr, HYPO71(revised): A computer program for determining hypocenter, magnitude and first-motion patterns of local earthquakes, *U. S. Geol. Surv. Open File Rep.*, *75-311*, 1975.

Oppenheimer, D. H., and K. E. Herkenhoff, Velocity-density properties of the lithosphere from three-dimensional modeling of The Geysers–Clear Lake region, California, *J. Geophys. Res.*, *86*, 6057–6065, 1981.

Pavlis, G. L., and J. R. Booker, Progressive multiple event location (PMEL), *Bull. Seismol. Soc. Am.*, *73*, 1753–1777, 1983.

Plouff, D., and W. F. Isherwood, Aeromagnetic and gravity surveys in the Coso Range, California, *J. Geophys. Res.*, *85*, 2491–2501, 1980.

Reasenberg, P., W. Ellsworth, and A. Walter, Teleseismic evidence for a low-velocity body under the Coso geothermal area, *J. Geophys. Res.*, *85*, 2471–2483, 1980.

Roquemore, G. R., Active faults and associated tectonic stress in the Coso Range, California, *Tech. Pap. 6270*, 101 pp., Nav. Weapons Cent., China Lake, Calif., 1981.

Roquemore, G. R., Ground magnetic survey in the Coso Range, California, *J. Geophys. Res.*, *89*, 3309–3314, 1984.

Roquemore, G. R., and J. T. Zellmer, Airport and Little Lake faults: Ground cracking associated with 1982 magnitude 5.2 Indian Wells Valley earthquake, Inyo County, *Calif. Geol.*, *36*, 977–200, 1983*a*.

Roquemore, G. R, and J. T. Zellmer, Tectonics, seismicity and volcanism at the Naval Weapons Center, *Nav. Res. Rev.*, *40*, 3–9, 1983*b*.

Savage, J. C., J. P. Church, and W. H. Prescott, Geodetic measurement of deformation in Owens Valley, California (abstract), *Geol. Soc. Am. Abstr. Programs*, *7*, 422, 1975.

Steeples, D. W., and H. M. Iyer, Low-velocity zone under Long Valley as determined from teleseismic events, *J. Geophys. Res.*, *81*, 849–860, 1976.

Stork, C., and R. W. Clayton, Iterative tomographic and migration reconstruction of seismic images, paper presented at Annual Meeting, Soc. of Explor. Geophys., Washington, D. C., Oct. 1985.

Walter, A. W., and C. S. Weaver, Seismicity of the Coso Range, California, *J. Geophys. Res.*, *85*, 2441–2458, 1980.

Weaver, C. S., and D. P. Hill, Earthquake swarms and local crustal spreading along major strike-slip faults in California, *Pure Appl. Geophys.*, *117*, 51–64, 1979.

Young, C.-Y., and R. W. Ward, Three-dimensional Q^{-1} model of the Coso Hot Springs known geothermal resource area, *J. Geophys. Res.*, *85*, 2459–2470, 1980.

Zbur, R. T., A geophysical investigation of Indian Wells Valley, California, *Tech. Pap. 2795*, 98 pp., U.S. Nav. Ord. Test Stn., China Lake, Calif., 1963.

R. W. Clayton, Seismological Laboratory, California Institute of Technology, Pasadena, CA 91125.

M. C. Walck, Geophysics Division 1541, Sandia National Laboratories, Albuquerque, NM 87185.

(Received December 30, 1985;
revised September 17, 1986;
accepted October 7, 1986.)